

SUPPLEMENTARY INFORMATION

Green synthesis of iron phosphide nanoparticles with high catalytic activity for liquid-phase nitrile hydrogenation

Tomohiro Tsuda,^a Shintaro Toyoda,^a Hiroya Ishikawa,^a Sho Yamaguchi,^{a,b} Tomoo Mizugaki^{a,b,c} and Takato Mitsudome^{*a,b,d}

^aDepartment of Materials Engineering Science, Graduate School of Engineering Science, Osaka University, 1-3 Machikaneyama, Toyonaka, Osaka, 560-8531, Japan

^bInnovative Catalysis Science Division, Institute for Open and Transdisciplinary Research Initiatives (ICS-OTRI), Osaka University, Suita, Osaka, 565-0871, Japan

^cResearch Center for Solar Energy Chemistry, Graduate School of Engineering Science, Osaka University, 1-3 Machikaneyama, Toyonaka, Osaka, 560-8531, Japan

^dPrecursory Research for Embryonic Science and Technology (PRESTO), Japan Science and Technology Agency (JST), 4-1-8 Honcho, Kawaguchi, Saitama, 333-0012, Japan

*Correspondence to: mitsudom@cheng.es.osaka-u.ac.jp

Table of Contents

1. General experimental details

2. Catalyst preparation

Scheme S1 Procedure of catalyst preparation.

3. Experimental procedure

4. Characterization and reaction study

Fig. S1 ATR-FTIR spectra of Fe–Ol, Fe–Er, Fe–St, and Fe–La.

Fig. S2 XRD patterns of samples synthesized with various iron precursors.

Fig. S3 A plausible reaction pathway for the hydrogenation of **1** to **2**.

Fig. S4 TEM image of Fe_xP–Ol after the reaction.

Fig. S5 XRD pattern of Fe_xP–Ol/TiO₂.

Fig. S6 TEM image of Fe_xP–Ol/TiO₂.

Fig. S7 Substrate scope of nitriles.

Table S1 Risks of iron and phosphorus reagents used in previous iron phosphide synthesis methods and our present approach.

Table S2 ICP-AES elemental analyses of Fe_xP–Ol and Fe_xP–Ol/TiO₂.

Table S3 Catalytic performances of various Fe_xP nanoparticles for hydrogenation of **1**.

Table S4 Comparison of activity between Fe_xP–Ol and reported iron-based heterogeneous catalysts for hydrogenation of **1**.

Table S5 Catalytic performances of Fe_xP–Ol prepared by different heating temperature.

5. Product identification

6. ¹H and ¹³C NMR spectra of product

7. Reference

1. General experimental details

All commercially available chemicals were used as received. Hexadecylamine (>95%), triphenylphosphite (>97%), diethylene glycol dimethyl ether (>99.0%), sodium oleate (>97.0%), sodium laurate (>97.0%), sodium stearate (>97.0%), erucic acid (>85.0%), iron(II) acetate (>90.0%), benzonitrile (>99.0%), and valeronitrile (>98%) were acquired from Tokyo Chemical Industry Co., Ltd (Tokyo, Japan). Sodium hydroxide (>97.0%), FeCl₃·6H₂O (>97.0%), iron(III) acetylacetonate (99%), ethanol (>99.5%), acetone (>99.0%), chloroform (>99.0%), hexane (>96.0%), 2-propanol (>99.5%), 4-cyanopyridine (>98%), 3-cyanopyridine (>98%), and 2-furancarboxitrile (>98%) were obtained from Fujifilm Wako Pure Chemical Corporation (Osaka, Japan). Iron(III) hydroxide oxide (95.0%) was purchased from Kanto Chemical Co., Ltd (Tokyo, Japan). TiO₂ (JRC-TIO-2) and Al₂O₃ (JRC-ALO-9) were provided by the Catalysis Society of Japan (Tokyo, Japan) as reference catalysts. SiO₂ (CARiACT, Q-6) was supplied by Fuji Silysia Chemical Ltd (Aichi, Japan).

Gas chromatography (GC) was conducted using a GC-2014 instrument (Shimadzu Corporation, Kyoto, Japan) equipped with a flame ionization detector and a capillary column (InertCap for amines, 30 m × 0.32 mm i.d., GL Sciences Inc., Tokyo, Japan). X-ray diffraction (XRD) studies were conducted on a Philips X'Pert-MPD diffractometer (Malvern Panalytical, Almelo, Netherlands) with Cu-K α radiation (45 kV, 40 mA). Attenuated total reflection Fourier transform infrared (ATR-FTIR) spectra were obtained using a IRSpirit-X (Shimadzu Corporation, Kyoto, Japan). Elemental analysis was performed using ICP-AES (Optima 8300, Perkin Elmer, Waltham, United States). ¹H and ¹³C nuclear magnetic resonance (NMR) spectra were recorded using a JNM-ESC400 spectrometer (JEOL Ltd., Tokyo, Japan). ¹H and ¹³C NMR chemical shifts were reported in parts per million (ppm) using the following standard chemical shifts: tetramethylsilane (0.00 ppm) for ¹H NMR; DMSO-*d*₆ (39.52 ppm) for ¹³C NMR. NMR multiplicities were reported using the following abbreviations: s: singlet, d: doublet, m: multiplet, *J*: coupling constants in hertz. Transmission electron microscopy (TEM) images were obtained using a Tecnai G2 20ST instrument (FEI Company, Hillsboro, United States) operated at 200 kV. Fe *K*-edge X-ray absorption fine structure (XAFS) measurements were conducted at room temperature at the BL01B1 line, using a Si (111) monochromator at SPring-8, Japan Synchrotron Radiation Research Institute (JASRI), Harima, Japan (2023B1646).

2. Catalyst preparation

● Synthesis of iron carboxylate complex

FeCl₃·6H₂O (2.4 mmol) was dissolved in distilled water (3.6 mL) in a round-bottom flask, and 8 mmol of sodium carboxylate (sodium oleate, sodium erucate, sodium stearate, and sodium laurate), ethanol (4.8 mL),

and hexane (8.4 mL) were added. The flask was purged with Ar gas, heated to 70 °C using an oil bath, and stirred at 500 rpm for 4 h. The organic phase was then washed with distilled water using a separatory funnel. After evaporating hexane in the organic phase, a waxy iron carboxylate complex (iron oleate (Fe–Ol), iron erucate (Fe–Er), iron stearate (Fe–St), and iron laurate (Fe–La)) was obtained, respectively.

- **Synthesis of sodium erucate**

Sodium hydroxide (12 mmol) and erucic acid (10 mmol) were dissolved in ethanol (40 mL) in a round-bottom flask and stirred at 500 rpm for 4 h at 40 °C. Subsequently, the obtained solid was washed with ethanol, filtered, and dried to obtain sodium erucate.

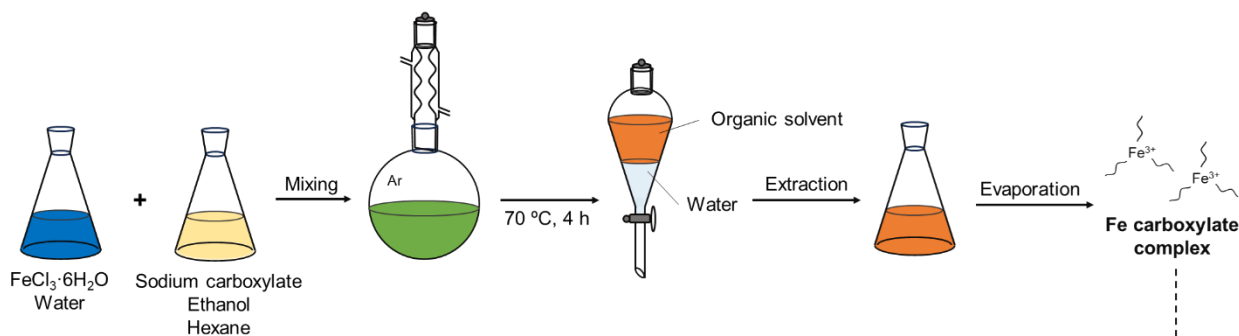
- **Synthesis of iron phosphide nanoparticles (Fe_xP)**

Triphenylphosphite (10 mmol) and hexadecylamine (10 mmol) were added to a Schlenk tube, and the mixture was stirred at 500 rpm under vacuum at 120 °C for 30 min. The 1 mmol of iron source (Fe–Ol, Fe–Er, Fe–St, Fe–La, and iron(II) acetate (Fe–Ac)) was then introduced, and the mixture was heated to 320 °C at a rate of 50 °C·min⁻¹ and stirred at 500 rpm for 4 h. The resulting black colloidal solution was centrifuged to collect the product, which was then washed with acetone and chloroform to obtain black nanoparticles (Fe_xP–Ol, Fe_xP–Er, Fe_xP–St, Fe_xP–La, and Fe_xP–Ac).

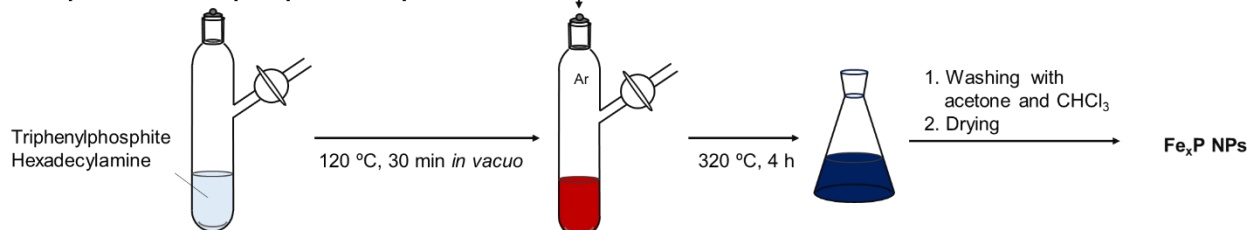
- **Synthesis of Fe_xP–Ol/TiO₂.**

Fe_xP–Ol (20 mg) was dispersed in chloroform (100 mL) and stirred at 500 rpm with TiO₂ (0.5 g) at 25 °C for 6 h to afford the corresponding Fe_xP–Ol/TiO₂.

a. Preparation of iron carboxylate complex



b. Preparation of iron phosphide nanoparticle



Scheme S1. Procedure of catalyst preparation. **a.** Preparation of iron carboxylate complex. **b.** Preparation of iron phosphide nanoparticle.

3. Experimental procedure

● Hydrogenation of benzonitrile (**1**) to benzylamine (**2**)

The typical reaction procedure for the hydrogenation of **1** using Fe_xP was as follows. Fe_xP (4 mg) was placed in a 50 mL stainless-steel autoclave with a Teflon inner cylinder, followed by the addition of **1** (0.5 mmol) and 2-propanol (2 mL). The reaction mixture was stirred at 180 °C under 3.8 MPa of H₂ and 0.2 MPa of NH₃ for 2 h. The reaction solution was analyzed by GC to determine the conversion, yield, and selectivity using diethylene glycol dimethyl ether as an internal standard. The conversion of **1**, yield and selectivity of **2**, yield of secondary imine (**1c**) as a byproduct, and turnover frequency (TOF) were calculated as follows (Eqs.1–5):

$$\text{Conversion (\%)} \text{ of } \mathbf{1} = \frac{\text{mol of substrate consumed after reaction}}{\text{initial mol of substrate}} \times 100\% \quad (1)$$

$$\text{Yield (\%)} \text{ of } \mathbf{2} = \frac{\text{mol of obtained primary amine product}}{\text{initial mol of substrate}} \times 100\% \quad (2)$$

$$\text{Selectivity (\%)} \text{ of } \mathbf{2} = \frac{\text{mol of obtained primary amine product}}{\text{mol of substrate consumed after reaction}} \times 100\% \quad (3)$$

$$\text{Yield (\%)} \text{ of } \mathbf{1c} = \frac{\text{mol of obtained secondary imine product}}{\text{initial mol of substrate}} \times 2 \times 100\% \quad (4)$$

$$\text{TOF (h}^{-1}\text{)} = \frac{\text{mol of obtained primary amine product}}{\text{mol of Fe used in the reaction} \times \text{reaction time}} \quad (5)$$

- **Product purification**

After the reaction, the reaction mixture was filtered to remove the catalyst, and the ammonia was removed by heating at 70 °C. The mixture was then added to a hydrogen chloride solution (1.25 M in 1,4-dioxane), and the solvent was removed to give the pure hydrochloride salt for NMR analysis.

4. Characterization and reaction study

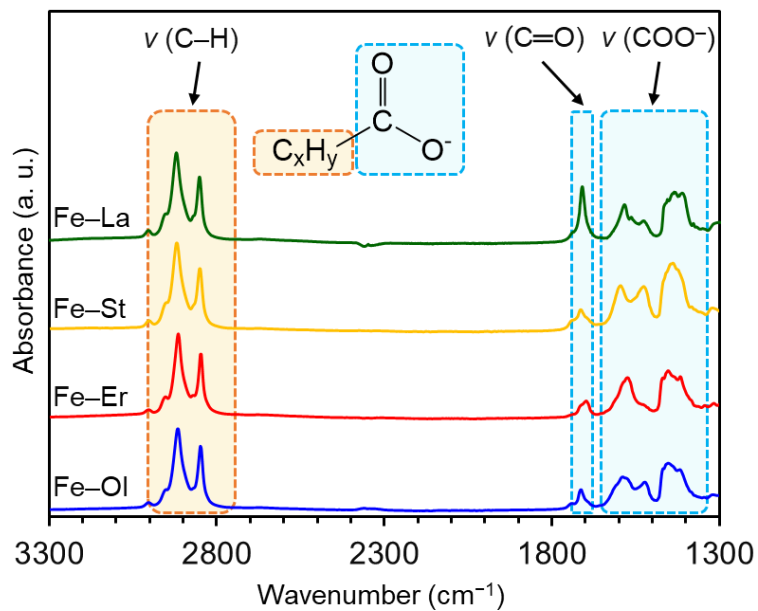


Fig. S1 ATR-FTIR spectra of Fe-OI, Fe-Er, Fe-St, and Fe-La.

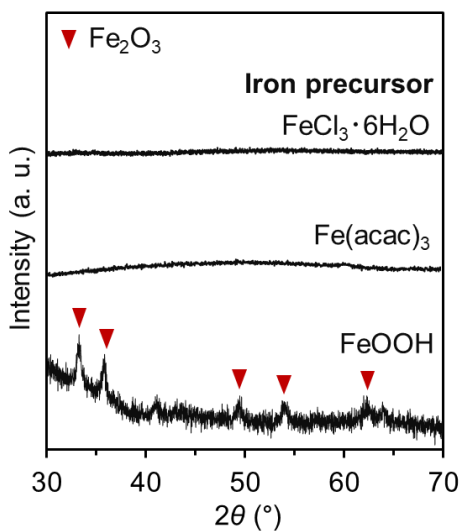


Fig. S2 XRD patterns of samples synthesized with various iron precursors.

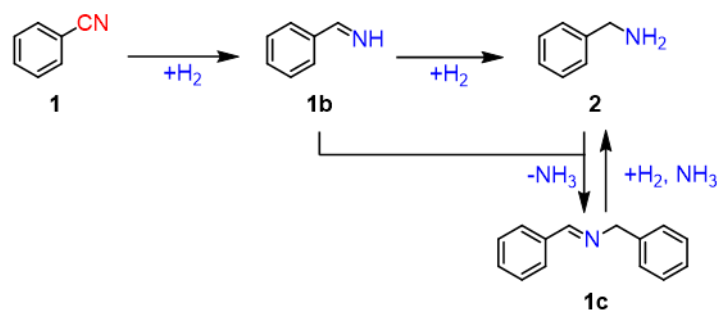


Fig. S3 A plausible reaction pathway for the hydrogenation of **1** to **2**.

First, the hydrogenation of **1** produces benzylideneamine (**1b**), which is then hydrogenated to yield **2**. Subsequently, **2** can condense with **1b** to form **1c**. This intermediate **1c** reacts with NH₃ and H₂ to produce **2** again.

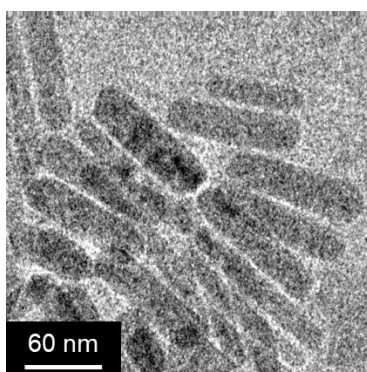


Fig. S4 TEM image of Fe_xP-OI after the reaction.

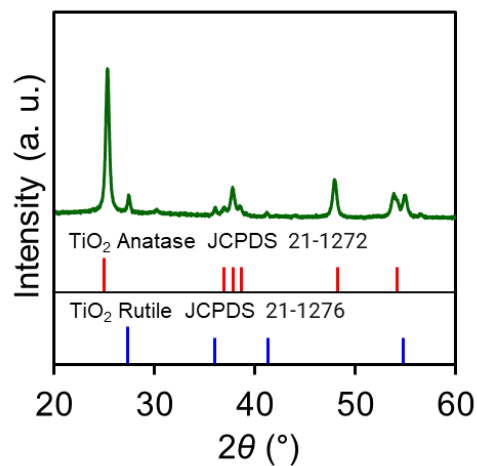


Fig. S5 XRD pattern of $\text{Fe}_x\text{P-OI/TiO}_2$.

XRD analysis of $\text{Fe}_2\text{P-OI/TiO}_2$ revealed only diffraction peaks corresponding to TiO_2 with rutile and anatase phases, suggesting that Fe_2P nanoparticles are highly dispersed.

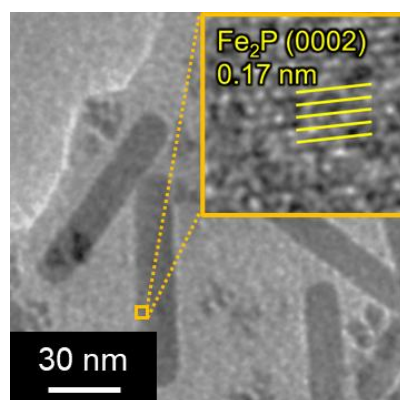


Fig. S6 TEM image of $\text{Fe}_x\text{P-OI/TiO}_2$. The inset shows high-resolution TEM image of $\text{Fe}_x\text{P-OI}$.

The images confirm that $\text{Fe}_2\text{P-OI}$ retains its rod-like structure upon deposition on TiO_2 and exhibits well-defined lattice fringes, which are consistent with the (0002) plane of hexagonal Fe_2P .

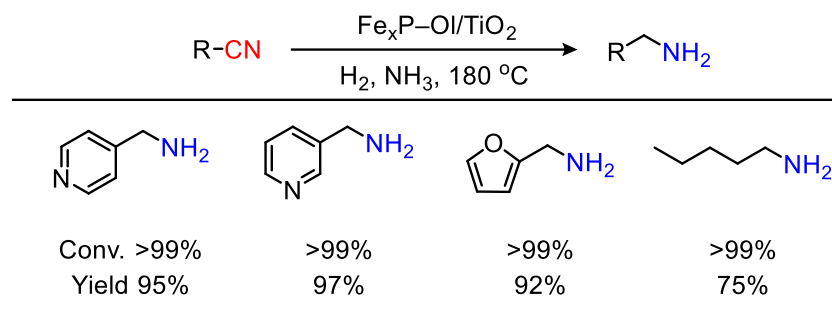


Fig. S7 Substrate scope of nitriles. Reaction conditions: $\text{Fe}_x\text{P-OI/TiO}_2$ (7.6 mol%), Substrate (0.5 mmol), 2-propanol (2 mL), H_2 gas (3.8 MPa), and NH_3 gas (0.2 MPa), 12 h. Conversion and yield were determined by GC using an internal standard technique.

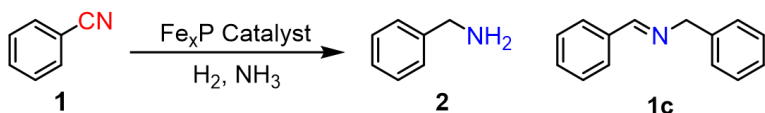
Table S1 Risks of iron and phosphorus reagents used in previous iron phosphide synthesis methods and our present approach.

Fe Precursor	P Source	Temp. (°C)	Product	Morphology	Risk	Ref.
Fe carboxylate	TPP	300–380	Fe ₂ P, FeP	Nanorods, Nanoparticles	N/A	This Work
Fe(CO) ₅	TOP	300	FeP	Nanorods, Wires	Fe(CO) ₅	S1
		300	Fe ₂ P	Nanorods, Wires	Air sensitivity High toxicity	S2
		360	FeP	Wires	TOP	S3
		350–380	Fe ₂ P, FeP	Nanorods, Nanoparticles	Air sensitivity Flammability	S4
	TPP	280–300	Fe ₂ P	Nanorods	Fe(CO) ₅	S5
		320	Fe ₂ P	Nanorods	Air sensitivity High toxicity	S6
FeCl ₃	Na ₃ P	190	FeP	Non-uniform shape	Na ₃ P	S7
		320	FeP	Non-uniform shape	Air sensitivity High toxicity	S8
Fe(acac) ₃	P(SiMe ₃) ₃	240	FeP	Nanoparticles	P(SiMe ₃) ₃ Air sensitivity Flammability	S9
FeOOH	TOP	320	FeP	Bundles	TOP Air sensitivity Flammability	S10

TPP = triphenylphosphite, TOP = trioctylphosphine

Table S2 ICP-AES elemental analyses of Fe_xP–OI and Fe_xP–OI/TiO₂.

Sample	Element	Amount (wt%)	Fe/P (molar ratio)
Fe _x P–OI	Fe	72.1	2.05
	P	19.4	
Fe _x P–OI/TiO ₂	Fe	2.28	1.92
	P	0.66	

Table S3 Catalytic performances of various Fe_xP nanoparticles for hydrogenation of **1**.


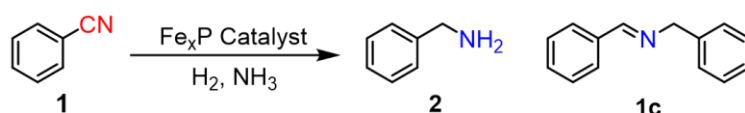
Entry	Catalyst	Conv. of 1 (%)	Yield of 2 (%)	Yield of 1c (%)
1	Fe _x P-OI	76	36 (47)	38
2	Fe _x P-OI/TiO ₂	>99	90 (90)	<1
3	Fe _x P-OI/Al ₂ O ₃	54	26 (48)	28
4	Fe _x P-OI/SiO ₂	52	25 (48)	24
5	Fe _x P-Er	1	1	<1
6	Fe _x P-St	1	1	<1
7	Fe _x P-La	26	14 (67)	12
8	Fe _x P-Ac	0	0	0
9	Fe ₂ P NC	35	19 (54)	16

Reaction conditions: Fe_xP (7.6 mol%), **1** (0.5 mmol), 2-propanol (2 mL), H₂ gas (3.8 MPa), NH₃ gas (0.2 MPa), 180 °C, and 2 h. Conversion, yield, and selectivity were determined by GC using an internal standard technique. The selectivity of **2** is denoted in parentheses.

Table S4 Comparison of activity between Fe_xP-OI and reported iron-based heterogeneous catalysts for hydrogenation of **1**.

Catalyst	Reaction conditions	TOF (h ⁻¹)	Ref.
Fe _x P-OI	7.6 mol% Fe, 3.8 MPa H ₂ , 0.2 MPa NH ₃ , 180 °C, 2 h.	2.37	This work
Fe ₂ P NCs	7.6 mol% Fe, 3.8 MPa H ₂ , 0.2 MPa NH ₃ , 180 °C, 2 h.	1.25	S6
Fe/Fe-O@SiO ₂	8.5 mol% Fe, 20 mol% Al foil, 5 MPa H ₂ , 0.5–0.7 MPa NH ₃ , 120 °C, 24 h.	0.47	S11

Table S5. Catalytic performances of Fe_xP–OI prepared by different heating temperatures.

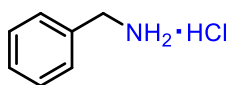


Entry	Heating Temp. (°C)	Composition	Conv. of 1 (%)	Yield of 2 (%)	Yield of 1c (%)
1	300	Fe ₂ P	31	11 (35)	16
2	320	Fe ₂ P	76	36 (47)	38
3	340	Fe ₂ P + FeP	28	12 (43)	14
4	360	Fe ₂ P + FeP	19	8 (42)	8
5	380	FeP	25	4 (16)	18

Reaction conditions: Fe_xP–OI (4 mg), **1** (0.5 mmol), 2-propanol (2 mL), H₂ gas (3.8 MPa), NH₃ gas (0.2 MPa), 180 °C, and 2 h. Conversion, yield, and selectivity were determined by GC using an internal standard technique. The selectivity of **2** is denoted in parentheses.

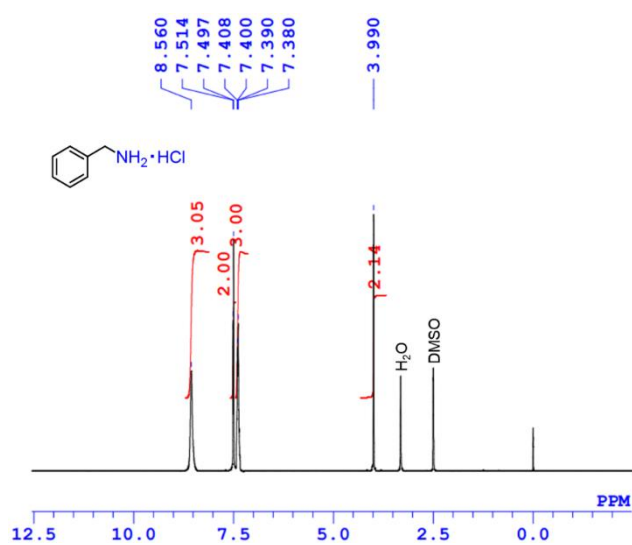
5. Product identification

benzylamine hydrochloride (2)

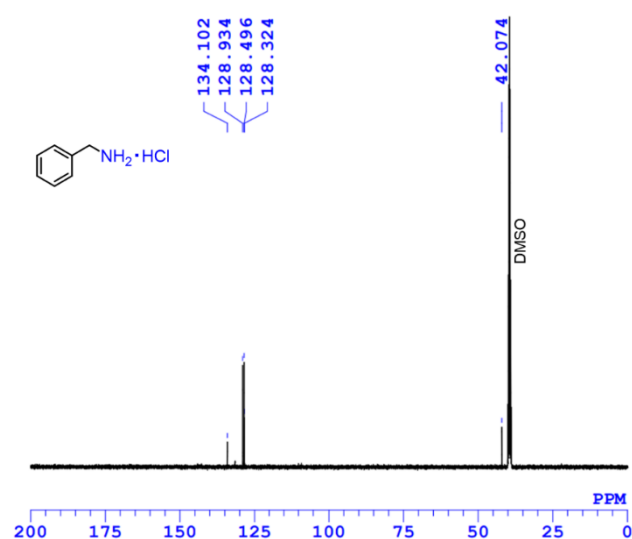


CAS registry No. [3287-99-8]. ^1H NMR (DMSO- d_6 , 400 MHz): $\delta = 8.56$ (s, 3H), 7.51 (d, $J = 6.8$ Hz, 2H), 7.41–7.38 (m, 3H), 3.99 (s, 2H); ^{13}C NMR (DMSO- d_6 , 100 MHz): $\delta = 134.10$, 128.93, 128.50, 128.32, 42.07.

6. ^1H and ^{13}C NMR spectra of product



^1H NMR spectrum of benzylamine hydrochloride (2)



^{13}C NMR spectrum of benzylamine hydrochloride (2)

7. Reference

- [S1] C. Qian, F. Kim, L. Ma, F. Tsui, P. Yang and J. Liu, *J. Am. Chem. Soc.*, 2004, **126**, 1195–1198.
- [S2] J. Park, B. Koo, Y. Hwang, C. Bae, K. An, J.-G. Park, H. M. Park and T. Hyeon, *Angew. Chem. Int. Ed.*, 2004, **43**, 2282–2285.
- [S3] J. Park, B. Koo, K. Y. Yoon, Y. Hwang, M. Kang, J.-G. Park and T. Hyeon, *J. Am. Chem. Soc.*, 2005, **127**, 8433–8440.
- [S4] E. Muthuswamy, P. R. Kharel, G. Lawes and S. L. Brock, *ACS Nano*, 2009, **3**, 2383–2393.
- [S5] J. Liu, M. Meyns, T. Zhang, J. Arbiol, A. Cabot and A. Shavel, *Chem. Mater.*, 2018, **30**, 1799–1807.
- [S6] T. Tsuda, M. Sheng, H. Ishikawa, S. Yamazoe, J. Yamasaki, M. Hirayama, S. Yamaguchi, T. Mizugaki and T. Mitsudome, *Nat. Commun.*, 2023, **14**, 5959.
- [S7] G. Yunle, G. Fan, Q. Yitai, Z. Huagui and Y. Ziping, *Mater. Res. Bull.*, 2002, **37**, 1101–1105.
- [S8] D. Ahluwalia, A. Varshney, S. Kumar, A. Kumar, S. G. Warkar, N. Singh and P. Dubey, *Inorg. Nano-Met. Chem.*, 2020, **50**, 1–6.
- [S9] S. C. Perera, P. S. Fodor, G. M. Tsoi, L. E. Wenger and S. L. Brock, *Chem. Mater.*, 2003, **15**, 4034–4038.
- [S10] M. Adhikari, S. Sharma, E. Echeverria, D. N. McIlroy and Y. Vasquez, *ACS Nanosci. Au*, 2023, **3**, 491–499.
- [S11] V. G. Chandrashekhar, T. Senthamarai, R. G. Kadam, O. Malina, J. Kašlík, R. Zbořil, M. B. Gawande, R. V. Jagadeesh and M. Beller, *Nat. Catal.*, 2022, **5**, 20–29.